Pump excited state absorption in holmium-doped fluoride glass

André Felipe Henriques Librantz,[1,2] Stuart D. Jackson,[3,a)] Laércio Gomes,[1] Sidney José Lima Ribeiro,[4] and Younes Messaddeq[4]
[1]*Center for Lasers and Applications, IPEN/CNEN-SP, P.O. Box 11049, São Paulo SP 05422-970, Brazil*
[2]*Sciences Department, UNINOVE, São Paulo SP 01156-050, Brazil*
[3]*Optical Fibre Technology Centre, University of Sydney, 206 National Innovation Centre, Australian Technology Park, Eveleigh 1430, Australia*
[4]*Institute of Chemistry-UNESP, P.O. Box 355, Araraquara SP 14801-970, Brazil*

(Received 23 September 2007; accepted 21 November 2007; published online 23 January 2008)

The primary excited state absorption processes relating to the $^5I_6 \rightarrow {}^5I_7$ 3 μm laser transition in singly Ho^{3+}-doped fluoride glass have been investigated in detail using time-resolved fluorescence spectroscopy. Selective laser excitation of the $^5I_6$ and $^5I_7$ energy levels established the occurrence of two excited state absorption transitions from these energy levels that compete with previously described energy transfer upconversion processes. The $^5I_7 \rightarrow {}^5I_4$ excited state absorption transition has peak cross sections at 1216 nm ($\sigma_{esa}=2.8\times10^{-21}$ cm^2), 1174 nm ($\sigma_{esa}=1\times10^{-21}$ cm^2), and 1134 nm ($\sigma_{esa}=7.4\times10^{-22}$ cm^2) which have a strong overlap with the $^5I_8 \rightarrow {}^5I_6$ ground state absorption. On the other hand, it was established that the excited state absorption transition $^5I_6 \rightarrow {}^5S_2$ had a weak overlap with ground state absorption. Using numerical solution of the rate equations, we show that Ho^{3+}-doped fluoride fiber lasers employing pumping at 1100 nm rely on excited state absorption from the lowest excited state of Ho^{3+} to maintain a population inversion and that energy transfer upconversion processes compete detrimentally with the excited state absorption processes in concentrated Ho^{3+}-doped fluoride glass. © *2008 American Institute of Physics*.
[DOI: 10.1063/1.2833436]

I. INTRODUCTION

Fiber lasers have made a significant impact in industry and research because of their capability of providing near diffraction-limited laser output in a compact, efficient, and, thus, cost effective device. The geometry and size of the fiber waveguide means that they are comparatively less affected by thermal problems and a high spatial quality output beam can typically be produced at very high output power levels.[1]

Many applications such as laser surgery[2–4] and remote sensing[5–7] are dependent on high power midinfrared radiation and, as a result, there exists a strong demand for the development of high power and efficient midinfrared laser devices. A midinfrared fiber laser that offers high power and high efficiency remains a technological challenge; however, a number of interesting and potentially power scalable midinfrared fiber laser alternatives, which operate at the short wavelength region of the midinfrared spectrum (at ~3 μm) have been demonstrated.[8–11]

The fluoride glasses based on the composition $ZrF_4-BaF_2-LaF_3-NaF$ (ZBLAN), which have the necessarily low maximum phonon energy, are currently the most developed host materials for midinfrared fiber lasers. Of the rare earth doped fiber lasers that have been tested for the generation of ~3 μm radiation, fluoride fiber lasers based on the $^5I_{11/2} \rightarrow {}^5I_{13/2}$ laser transition of the Er^{3+} ion producing ~2.7 μm laser radiation have presented the highest output power.[12] On the other hand, the emission wavelength (of between 2.84 and 2.86 μm) relevant to the $^5I_6 \rightarrow {}^5I_7$ laser transition of Ho^{3+} overlaps well with the fundamental vibration of the OH bond, and the potentially improved power scalability of midinfrared Ho^{3+}-based ZBLAN fiber lasers compared to Er^{3+}-doped ZBLAN fiber lasers has instigated further research.

Past demonstrations of midinfrared Ho^{3+}-doped ZBLAN fiber lasers have involved excitation with the use of either Yb^{3+}-doped silica fiber lasers operating at 1.1 μm,[11,13] or Raman fiber lasers pumped operating at 1.15 μm.[14] These versatile approaches to the excitation of midinfrared fiber lasers have allowed the demonstration of alternative midinfrared fiber lasers including the Dy^{3+}-doped ZBLAN fiber laser.[15] But, in a similar way to the Er^{3+} ion transition, the lifetime of the lower laser level of the Ho^{3+} ion is longer (12 ms) compared to the 3.5 ms lifetime of the upper laser level. As a result, the demonstration of ~2.5 W from a Ho^{3+}-doped ZBLAN fiber laser[11] required Pr^{3+} ion desensitization in order to reduce population bottlenecking at the lower $^5I_7$ laser level.

Recently,[16] we identified and quantified a range of energy transfer upconversion (ETU) processes that involve the $^5I_6$ and $^5I_7$ energy levels of Ho^{3+} in singly Ho^{3+}-doped ZBLAN glass. In contrast to demonstrations requiring desensitization, the production of 340 mW output power from a high concentration (4.2 mol %) singly Ho^{3+}-doped ZBLAN fiber laser[13] was thought to relate to one of these ETU processes that acts to reduce the electron population in the lower laser level and repopulate the upper laser level. In this investigation, we extend this work by identifying and quantifying a range of pump excited state absorption (ESA) processes that affect the functioning of Ho^{3+}-doped ZBLAN fiber la-

a)Electronic mail: s.jackson@oftc.usyd.edu.au.

TABLE I. Luminescence branching ratio, and experimental and radiative lifetimes of Ho^{3+} used in the rate equations.

Luminescence branching ratio and radiative lifetimes of Ho^{3+}[a]				
Transition	β	τ_R	τ(exp) ($[Ho^{3+}]$=4 mol %)[b]	W_{nr} (s^{-1})
$^5S_2\rightarrow$		340 μs	300 μs	392
$^5I_6$	0.06		(21 μs)	
$^5I_7$ (741 nm)	0.34			
$^5I_8$ (538 nm)	0.61			
$^5F_5\rightarrow$		17 ms	50 μs	19941
$^5I_7$ (1162 nm)	0.55			
$^5I_8$ (899 nm)	0.41			
$^5I_6\rightarrow$		5.9 ms	3.5 ms	116.2
$^5I_7$ (2889 nm)	0.09		(4.6 ms)	
$^5I_8$ (1168 nm)	0.91			
$^5I_7\rightarrow$		12.6 ms	12 ms	
$^5I_8$ (1960 nm)	1		(31.8 ms)	

$Ho^{3+}-Ho^{3+}$ energy transfer rates constants[c]				
Ho^{3+} (4 mol %) Process	I (ions cm^{-3}) (excitation density)	K_{ETU} (s^{-1})	K_0 (s^{-1})	W_{CR} (s^{-1})
ETU1	1.6×10^{18} cm^{-3}	70	72	⋯
ETU2	3.4×10^{18} cm^{-3}	623	650	⋯
CR1		⋯		19487
CR2				43859

[a]Values obtained from the literature (Ref. 20).
[b]Experimental lifetimes obtained in this work.
[c]Experimental lifetimes and calculated rate values (Ref. 15).

sers operating on the midinfrared $^5I_6\rightarrow{}^5I_7$ laser transition. We show, using a numerical model, that correctly predicts the performance of Ho^{3+}-doped ZBLAN fiber lasers pumped at 1.1 μm that pump ESA processes are primarily responsible for the recycling of energy back to the upper laser level.

II. EXPERIMENTAL PROCEDURE

The Ho^{3+}-doped ZBLAN glass samples used for the time-resolved luminescence spectroscopy measurements were prepared from ultrapure fluoride starting materials in the composition $(100-x)$ $(53ZrF_4-20BaF_2-4LaF_3-20NaF)-xHoF_3$ (x=4 mol %). The starting powder materials were melted at 850 °C for 120 min in a Pt–Au crucible. The liquids were poured into brass molds and annealed at 260 °C for 2 h to remove the mechanical stresses. The samples were cut and polished into $15\times10\times5$ mm^3 pieces.

Absorption spectra in the range of 300–2000 nm were measured using a spectrophotometer (Cary/OLIS 17D). The decay characteristics of the excited states of Ho^{3+} were measured using pulsed (4 ns) laser excitation from a tunable optical parametric oscillator (OPO) pumped by the second harmonic of a Q-switched neodymium-doped yttrium aluminum garnet (Nd-YAG) laser (Brilliant B from Quantel). Tunable laser excitation from the OPO was used to excite the $^5I_6$ and $^5I_7$ energy levels directly. The luminescence was detected using an S-20 photomultiplier tube (EMI, refrigerated to −20 °C) using a shunt resistance of 50 Ω (anode pulse rise time of 10 ns) and analyzed using a digital 200 MHz oscilloscope (Tektronix TDS 410). The luminescence signals in the visible to near infrared region were isolated using a 0.25 m monochromator (KRATOS) containing a dispersion grating with 1200 grooves mm^{-1}. All the fluorescence decay characteristics were measured at 300 K.

III. EXPERIMENTAL RESULTS

Time resolved luminescence spectroscopy using selective pulsed laser excitation in the wavelength range of 1110–1220 nm was used to investigate the upconversion processes involving the $^5I_6$ and $^5I_7$ levels. These upconversion processes relate to either pump ESA in which the $^5I_6$ or $^5I_7$ levels absorb pump photons or ETU via nonradiative energy transfer between the excited $^5I_6$ or $^5I_7$ levels. These ETU processes have been investigated in detail in a previous investigation[16] and the experimental and the radiative lifetimes of the $^5S_2$, $^5F_5$, $^5I_5$, $^5I_6$, and $^5I_7$ levels of Ho^{3+} are shown in Table I. Included in Table I are the rates of the relevant ETU processes $Ho^{3+}(^5I_7,{}^5I_7)\rightarrow Ho^{3+}(^5I_6,{}^5I_8)$, labeled ETU1, and $Ho^{3+}(^5I_6,{}^5I_6)\rightarrow Ho^{3+}(^5F_5,{}^5I_8)$, labeled ETU2, and the cross relaxation process $Ho^{3+}(^5F_5,{}^5I_8)\rightarrow Ho^{3+}(^5I_6,{}^5I_7)$ which is labeled CR1.

A. Pump excited state absorption from the $^5I_6$ level

Figure 1 displays the emission response at a wavelength of 545 nm after short pulse laser excitation at 1151 nm. This emission relates to the decay of the $^5S_2$ level and it exhibits a fast rise time comparable with the ~10 ns response time of the detection system. The decay time of the $^5S_2$ state in Ho^{3+}

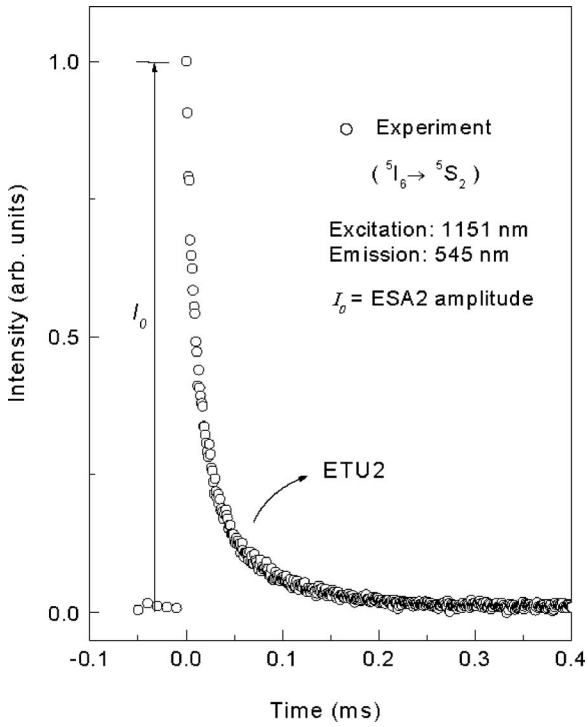

FIG. 1. Measured luminescence characteristic of the $^5S_2$ excited state of Ho^{3+} measured at 545 nm after laser excitation with 4 ns, 10 mJ (10 Hz) pulses at 1151 nm.

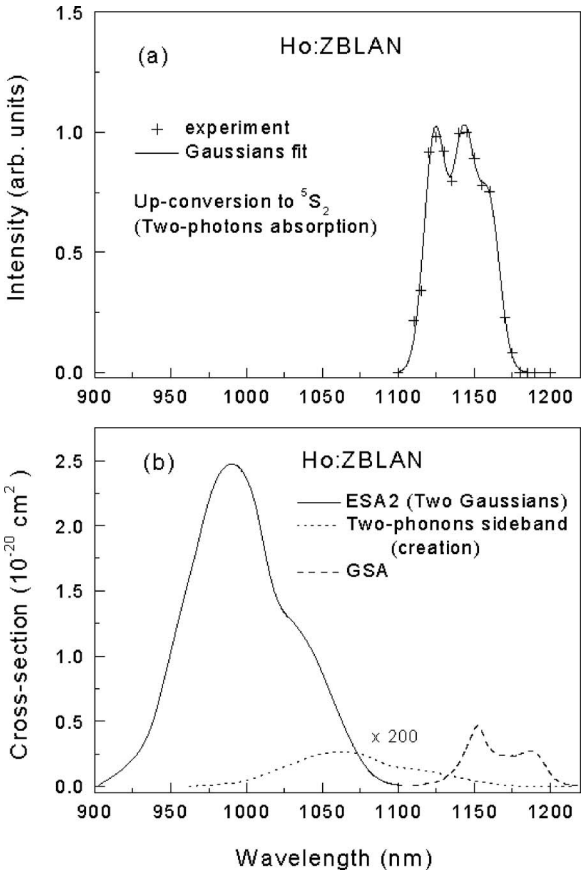

FIG. 2. (a) Measurements of the excitation spectrum for emission at 545 nm from the $^5S_2$ level after pulsed laser excitation that was tuned to the $^5I_8 \rightarrow {}^5I_6$ GSA transition. Crosses are the experimental data and the solid line is a least-squares fit using three Gaussian functions. (b) The solid line represents the calculated cross section of the ESA2 process using two superimposed Gaussian functions which were scaled by the radiative rate of the $^5S_2$ level (τ_R=300 μs). The dotted line represents the calculated two-phonon absorption sideband and the dashed line is the measured GSA.

(0.1 mol %)-doped ZBLAN was 300 μs that decreased to 21 μs in Ho^{3+} (4 mol %)-doped ZBLAN due to the $Ho^{3+}(^5S_2, ^5I_8) \rightarrow Ho^{3+}(^5I_4, ^5I_7)$ nonradiative cross relaxation decay process, which we label CR2, as verified by exciting it directly with photons at a wavelength of 532 nm.[16] We interpret the green emission as being produced by pump photon absorption by way of the ESA process $^5I_6 \rightarrow {}^5S_2$, which we label ESA2. Assigning the emission intensity just after the pump pulse (at $t \sim 0$) the initial amplitude of the green emission, I_0, we can plot the values for I_0 as a function of pump wavelength, as shown in Fig. 2(a). The two-photon absorption process is represented by (i) $^5I_8 + h\nu_P \rightarrow {}^5I_6$ and (ii) $^5I_6 + h\nu_P \rightarrow {}^5S_2$; the absorption of the second pump photon is nonresonant.

The solid line in Fig. 2(a) was obtained using a least-squares fit to the experimental data with three Gaussian functions: the peak positions of the functions occurring at 1126, 1144, and 1158 nm. We chose to use Gaussian functions for the decomposition of the 545 nm excitation spectrum because these functions have been used to describe the absorption and emission transitions between electronic levels of ions in solids that have a random distribution of the local electric fields at the ion sites.[17] The ground state absorption (GSA) spectrum is shown in Fig. 2(b). It can be observed that the two-photon absorption process, which leads to the emission of 545 nm luminescence, does not follow the GSA spectrum; the main peak in the GSA spectrum occurs at a wavelength of 1151 nm.

B. Pump excited state absorption from the $^5I_7$ level

Evidence that the $^5I_4$ and $^5I_5$ energy levels of Ho^{3+} are excited after laser excitation of a Ho^{3+} (4.2 mol %)-doped ZBLAN fiber laser at wavelengths near 1100 nm was shown in the visible spectrum emitted from the fiber.[13] In the present investigation, we could observe the upconverted luminescence at 899 nm which results from fluorescence from the $^5I_5$ level when exciting the $^5I_8 \rightarrow {}^5I_6$ GSA transition with our short pulse probe light. Figure 3(a) shows the weak 899 nm emission response induced by the probe pulses at 1180 nm. As can be observed in Fig. 3(b), the luminescence comprises of two separate rise times; the first with a rise time of $\sim$1 μs due to $^5I_4$ excited level decay which is comparatively fast because the $^5I_4$ level decays nonradiatively by way of multiphonon emission and a second slower rise time of $\sim$50 μs that is well-matched with the expected lifetime of the $^5I_5$ level at room temperature.[18] The overall process can be represented by (i) $^5I_8 + h\nu_P \rightarrow {}^5I_6$; (ii) $^5I_6 \rightarrow {}^5I_7 + h\nu$ (2.9 μm); (iii) $^5I_7 + h\nu_P \rightarrow {}^5I_4 \rightarrow {}^5I_5 + \hbar\omega$ (phonons). The long decay time of the 899 nm emission observed in Fig. 3(a) is consistent with the mean decay time of $\sim$6.83 ms measured for the $^5F_5$ level[16] in Ho^{3+} (4 mol %)-doped ZBLAN glass which is excited by the ETU2 process after the $^5I_6$ level is populated by GSA: the $^5I_5$ level is populated after multiphonon decay from the $^5F_5$ level through the $^5I_4$ level.

The initial amplitude I_0 of the 899 nm emission was measured $\sim$2 μs after the probe pulse in order to isolate the

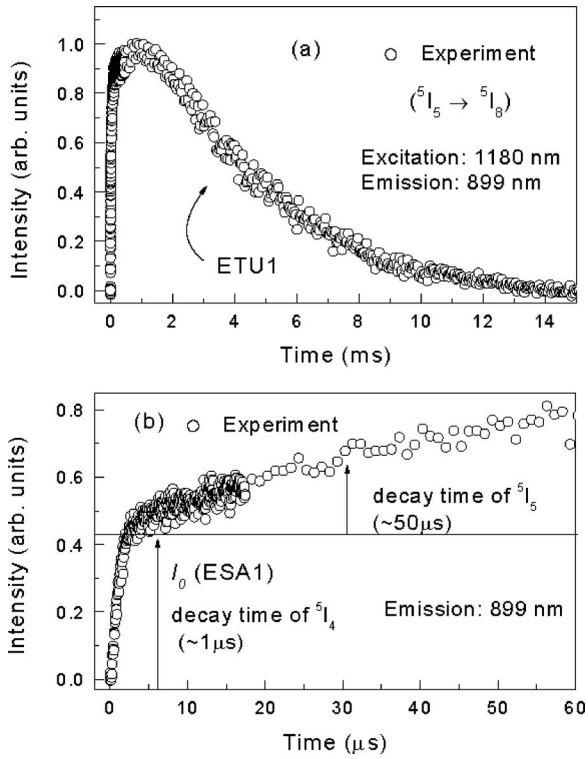

FIG. 3. Measured (a) luminescence characteristic at 899 nm from the $^5I_5$ level after laser excitation with 4 ns, 10 mJ (10 Hz) pulses at 1180 nm. The long decay time (of ~7 ms) is due to the long decay of the $^5F_5$ excited state that is populated by ETU1 and (b) detail of the temporal characteristic of the 899 nm emission in the 0–60 μs range.

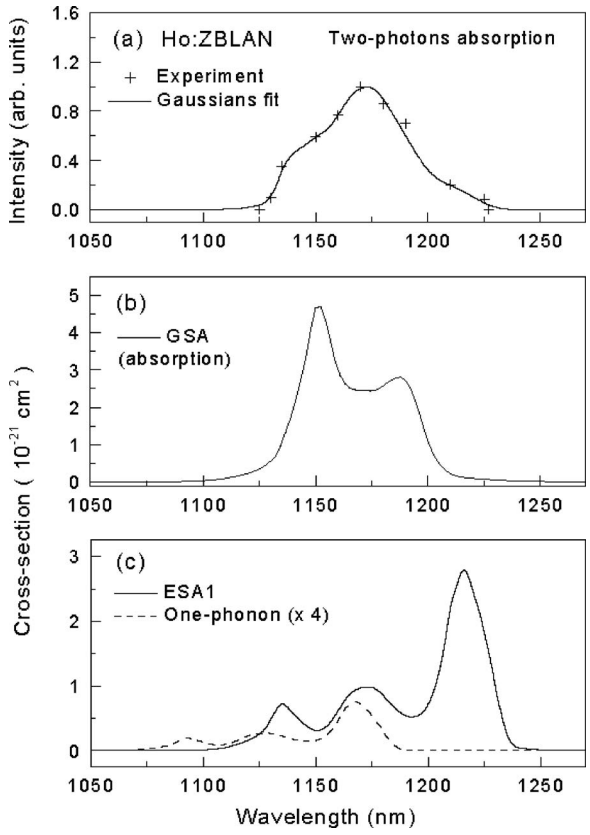

FIG. 4. Measured (a) excitation spectrum (crosses) of the 899 nm emission intensity I_0 measured 2 μs after the probe pulses which were tuned from 1110 to 1220 nm and (b) cross section of the GSA spectrum of the $^5I_8 \rightarrow {}^5I_6$ transition. (c) Calculated cross section for the ESA1 transition (solid line) and the calculated one-phonon sideband (dotted line).

contribution from ESA for a range of probe wavelengths tuned over the $^5I_8 \rightarrow {}^5I_6$ GSA transition of Ho^{3+}. Figure 4(a) shows the values (crosses) of I_0 as a function of the probe wavelength and the solid line in Fig. 4(a) represents the best fit to the experimental data using a least-squares fit comprising three Gaussian functions which are centered at 1145, 1175, and 1215 nm. It can be observed that the two-photon excitation band follows approximately with the GSA spectrum shown in Fig. 4(b). By inspection of the minimum and maximum energies of $^5I_7 \rightarrow {}^5I_4$ transition of Ho^{3+} in ZBLAN, it can be deduced that the ESA1 spectrum will occur in the range covered by the two-photon excitation spectrum. One may obtain the ESA1 spectrum [or $S(\lambda)$] by means of the normalized two-photon absorption (TPA) and GSA spectra using the following relation:

$$S(\lambda) = \frac{\mathrm{TPA}(\lambda)}{\mathrm{GSA}(\lambda)}. \tag{1}$$

The solid line in Fig. 4(c) shows the cross section of the ESA1 process using Eq. (1).

C. Calculation of the ESA cross sections

Using the Judd-Ofelt theory it is possible to estimate the ESA1 cross section. The rate of spontaneous emission from ^5I_J state for an electric dipole transition is given by[19]

$$A^{\mathrm{ed}}(J,J') = \frac{64\pi^4 e^2 \chi}{3h\lambda^3} S^{\mathrm{ed}}, \tag{2}$$

where $S^{\mathrm{ed}} = [1/(2J+1)]\Sigma_{\lambda=2,4,6}\Omega_\lambda |\langle U^{(\lambda)}\rangle|^2$ and $\chi = n(n^2+2)^2/9$. The spectroscopic intensity parameters Ω_2, Ω_4, and Ω_6 are equal to 230×10^{-22}, 230×10^{-22}, and 171×10^{-22} cm^2, respectively, for Ho^{3+}-doped ZBLAN.[20] Values of $|\langle U^{(\lambda)}\rangle|^2$ were obtained from the literature[19] for all the radiative transitions from the $^5I_4$ excited state of Ho^{3+} are listed in Table II. The refractive index $n=1.45$ for ZBLAN. The absorption cross section spectrum due to $^5I_7 \rightarrow {}^5I_4$ transition (or ESA1 band) was calculated using Eq. (2) and $\bar{\lambda}$

TABLE II. Values of the matrix elements of the unit angular tensor operator $|\langle U^{(\lambda)}\rangle|^2$. [These values were obtained from the literature (Ref. 19) for the radiative transitions from $^5I_4$ excited state of Ho^{3+}. The calculated radiative lifetime of $^5I_4$ state in Ho^{3+}-doped ZBLAN was 14.3 ms. The measured one was 1 μs and the luminescence efficiency was observed to be equal to 7×10^{-5}.]

Transition $\bar{\lambda}$ (nm)	$\lvert\langle U^{(2)}\rangle\rvert^2$	$\lvert\langle U^{(4)}\rangle\rvert^2$	$\lvert\langle U^{(6)}\rangle\rvert^2$	A^{ed} (s^{-1})
$^5I_4 \rightarrow {}^5I_5$ (4472)	0.0312	0.1237	0.9099	0.33
$^5I_4 \rightarrow {}^5I_6$ (2064)	0.0022	0.0281	0.6640	29.7
$^5I_4 \rightarrow {}^5I_7$ (1211)	0.0000	0.0033	0.1568	33.2
$^5I_4 \rightarrow {}^5I_8$ (749)	0.0000	0.0000	0.0077	6.8

$=1211$ nm (average excitation wavelength or centroid), $\int S(\lambda)d\lambda=43.5$ nm (integrated line shape), and $\Sigma_{J'}A_{J'}^{\mathrm{ed}}=70.4\ \mathrm{s}^{-1}$ [the total radiative decay rate of the $^5I_4$ excited state calculated using Eq. (2)]. The absorption cross section is given by

$$\sigma_{i\to f}^{\mathrm{abs}}(\lambda)=\frac{\bar{\lambda}^4}{8\pi c}\frac{g_f}{g_i}\left(\sum_{J'}A_{J'}^{\mathrm{ed}}\right)\frac{S(\lambda)}{\int S(\lambda)d\lambda}, \tag{3}$$

where $g=2J+1$ (i for the initial and f for the final states), $S(\lambda)$ is the line shape of the ESA spectrum, and c the speed of light. The maximum cross section for ESA1 is equal to 2.35×10^{-21} cm^2 at $\lambda=1216$ nm, which corresponds to approximately 1/2 of the maximum cross section for GSA, which is 4.7×10^{-21} cm^2 at $\lambda=1149$ nm. The resultant ESA1 band was calculated using Eq. (1) providing the spectrum shown in Fig. 4(c). The ground state absorption (GSA) is shown in Fig. 4(b) for comparison with the ESA1 band.

The crucial result from this work is that the ESA processes, ESA1 and ESA2, directly excite $^5I_4$ and $^5S_2$ levels, respectively, when Ho^{3+}-doped ZBLAN glass is pumped on the GSA process $^5I_8\to{}^5I_6$. The 1100 nm pump wavelength,[13] however, is outside the excitation spectrum arising from TPA, as shown Figs. 2(a) and 4(a). Thus, the visible emission that was observed in Ref. 13 suggests that the ESA1 and ESA2 processes must have been assisted by the phonons of the glass. For a complete description, the ESA cross sections and ESA spectral line shapes including the phonon sidebands must be taken into account to determine the contribution of the ESA processes to the 3 μm fiber laser.

The dashed line in Fig. 4(c) shows the one-phonon sideband of ESA1, i.e., the ESA transition assisted by one-phonon annihilation. The sideband spectrum was calculated using the method employed in Ref. 21, which is based on the fact that the phonon sideband results from an optical transition coupled to the local phonon field, whereby phonons are created to produce a high energy sideband or they are annihilated to produce a low energy sideband. In the case of excitation at 1100 nm, the ESA1 process is completed when one or two phonons are absorbed from the glass. In this case, the sideband is obtained by means of ESA1(λ) spectrum by shifting the wavelength λ to λ_k^- according to the relation $\lambda_k^-=(1/\lambda-k\hbar\omega)^{-1}$, where $k\hbar\omega$ is the total (phonon) energy absorbed from the lattice. The sideband amplitude must be scaled using the k-phonon annihilation probability P_k^- that is given by $P_k^-\cong\exp(-2\bar{n}S_0)(S_0^k/k!)(\bar{n})^k$, where $\bar{n}=[\exp(\hbar\omega/KT)-1]^{-1}$ is the occupation number of the phonon mode (at $T=300$ K). $S_0\sim0.31$ is the electron-phonon coupling (or Huang-Rhys factor) and $\hbar\omega=330\ \mathrm{cm}^{-1}$ is the average phonon energy of all the phonon modes which are coupled to the multiphonon sideband absorption relevant to ZBLAN glass.[22] The one-phonon sideband was obtained according to the following relation: $SB(\lambda_1^-)=P_1^-\mathrm{ESA1}(\lambda\to\lambda_1^-)$, where $P_1^-=0.068$. Figure 4(c) shows the high energy sideband spectrum and it indicates that one ($k=1$) phonon annihilation is necessary to activate the ESA1 process when the pump wavelength is 1100 nm.

The same approach was employed for the determination of the ESA2 sideband spectrum. Using the energy level diagram of Ho^{3+} in ZBLAN glass,[20] one expects two primary absorption transitions comprising the $^5I_6\to{}^5S_2$ absorption when one considers the Stark sublevel structure of these energy levels in Ho^{3+}-doped ZBLAN glass: the first transition with a peak p1 at 997 nm with a half-width (H) of 54 nm and a second transition with a peak p2 at 1030 nm with $H=34$ nm. The absorption spectrum of ESA2 was calculated using two superposed Gaussian functions and the Boltzmann distribution applied to the two distinguishable Stark levels of the I_6 level (at $T=300$ K) to scale the contribution of each transition to the total ESA2 absorption spectrum. Integration of the ESA2 spectrum gave $\int S(\lambda)d\lambda=64$ nm and $\bar{\lambda}=1010$ nm. Using the total radiative rate of the $^5S_2$ level, $\Sigma_{J'}A_{J'}^{\mathrm{ed}}=3334\ \mathrm{s}^{-1}$ (Ref. 20) in Eq. (3), we obtained the absorption cross section spectrum of ESA2, see solid line in Fig. 2(b). By inspecting this spectrum, one can conclude that a phonon sideband that involves one- or two-phonon emission accounts for the ESA that would take place under laser excitation at 1100 nm. The two-phonon sideband was obtained by translating the ESA2(λ) spectrum using the relation $\lambda_k^+=[1/\lambda+k\hbar\omega]^{-1}$ (where $k=2$). The amplitude was scaled using the two-phonon emission probability given by $P_k^+\cong\exp[-(2\bar{n}+1)S_0](S_0^k/k!)(\bar{n}+1)^k$, where $k=2$ and, hence, $P_2^+=0.048$. The two-phonon sideband was calculated using the relation $SB(\lambda_2^+)=P_2^+\mathrm{ESA2}(\lambda\to\lambda_2^+)$, whose spectrum is shown by the dotted line in Fig. 2(b). Comparing the results in Figs. 2(b) and 4(c), one can state that in order to produce ESA from the $^5I_6$ level with a pump wavelength of 1100 nm, the emission of two phonons is necessary and the estimated ESA cross section is $\sim2.72\times10^{-23}$ cm^2. On the other hand, the absorption of one phonon is necessary for ESA to take place from the $^5I_7$ level and the ESA cross section is $\sim4.7\times10^{-23}$ cm^2.

IV. DISCUSSION

Recently,[23] it has been suggested that ESA, specifically ESA1 in the current investigation, was crucial to the operation of a Ho^{3+}-doped ZBLAN fiber laser operating on the $^5I_6\to{}^5I_7$ transition. The authors reported a high slope efficiency of 45%, despite the Stokes efficiency limit of 40%, when the fiber was excited at 1175 nm. The low [Ho^{3+}] of 0.5 mol % in this fiber precluded strong rates of ETU and, therefore, ESA may have provided the energy recycling required to produce the pump-limited output power of 650 mW. These results must be compared to the earlier demonstration of an output power of 340 mW at 2.92 μm from a Ho^{3+} (4.2 mol %)-doped ZBLAN fiber laser that produced 5% slope efficiency when excited at 1100 nm. Thus, a numerical simulation of these fiber lasers is necessary to elucidate the underlying mechanisms underpinning the performance of these Ho^{3+}-doped ZBLAN fiber laser systems.

A. Rate equations for optical excitation of the $^5I_6$ level

Figure 5 shows the simplified energy level scheme used to describe the Ho^{3+}-doped ZBLAN laser system for cw laser pumping the n_3 level ($^5I_6$). n_1, n_2, n_3, n_4, and n_5 are the $^5I_8$,

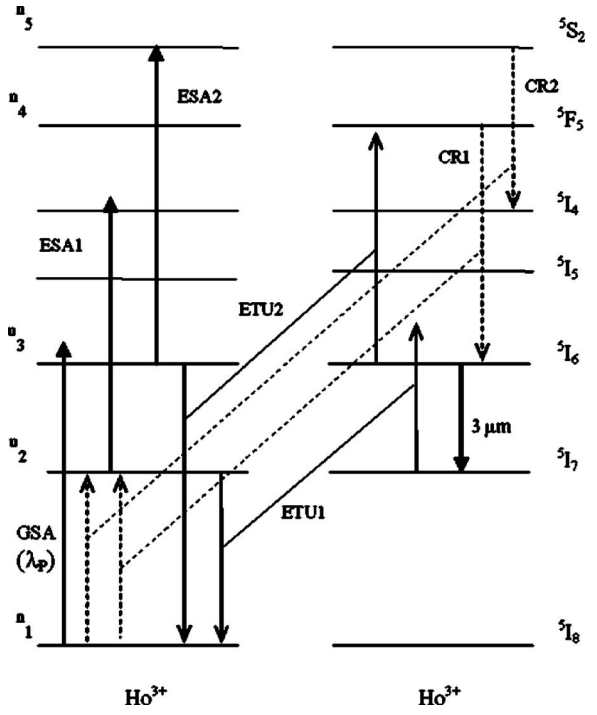

FIG. 5. Simplified energy level diagram for the Ho^{3+} ion showing the ground state absorption (GSA), excited state absorption (ESA), energy transfer upconversion (ETU), and cross relaxation (CR) processes.

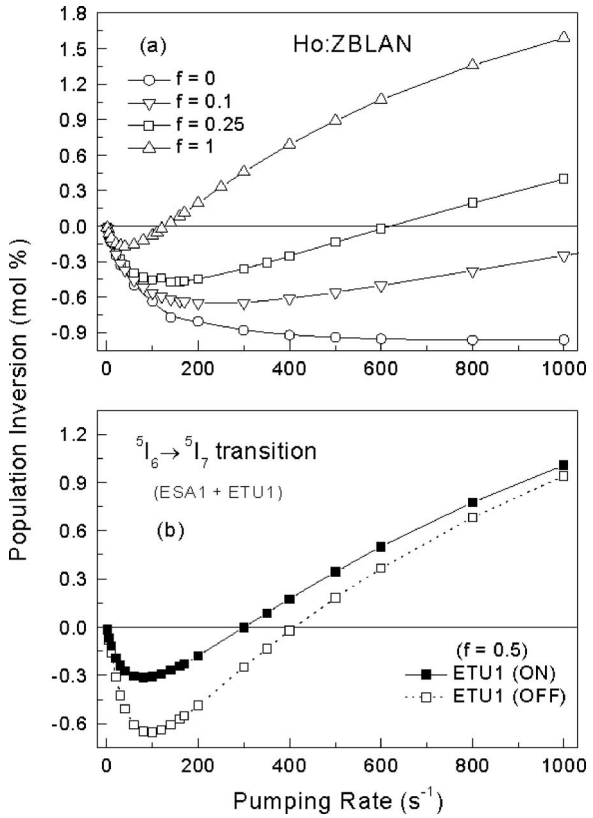

FIG. 6. Calculated steady state population inversion (n_3-n_2) as a function of the pump rate and as a function of (a) f, the cross section ratio, and (b) of the contribution from ETU1 where f=0.5.

$^5I_7$, $^5I_6$, $^5F_5$, and $^5S_2$ populations of Ho^{3+}, respectively, and $n_1+n_2+n_3+n_4+n_5=1$. The rate equations for the system are

$$\frac{dn_1}{dt} = -R_P n_1 + \frac{n_2}{\tau_2} + \frac{B_{31}}{\tau_{R_3}} n_3 - W_{\mathrm{CR1}} n_1 n_4 + K_{\mathrm{ETU2}} n_3^2 + \frac{\beta_{41}}{\tau_{R_4}} n_4 + K_{\mathrm{ETU1}} n_2^2 + \frac{\beta_{51}}{\tau_{R5}} n_5 - W_{\mathrm{CR2}} n_1 n_5, \quad (4)$$

$$\frac{dn_2}{dt} = W_{\mathrm{CR1}} n_1 n_4 + \left(\frac{B_{32}}{\tau_{R_3}} + W_{\mathrm{nR}}(32) \right) n_3 - \frac{n_2}{\tau_2} + \frac{\beta_{42}}{\tau_{R_4}} n_4 - 2K_{\mathrm{ETU1}} n_2^2 + \frac{\beta_{52}}{\tau_{R5}} n_5 - K_{\mathrm{ESA1}} n_2 + W_{\mathrm{CR2}} n_1 n_5, \quad (5)$$

$$\frac{dn_3}{dt} = R_P n_1 + W_{\mathrm{CR1}} n_1 n_4 - \frac{n_3}{\tau_3} - 2K_{\mathrm{ETU2}} n_3^2 + \left(\frac{\beta_{43}}{\tau_{R_4}} + W_{\mathrm{nR}}(43) \right) n_4 + K_{\mathrm{ESA1}} n_2 - K_{\mathrm{ESA2}} n_3 + W_{\mathrm{CR2}} n_1 n_5, \quad (6)$$

$$\frac{dn_4}{dt} = K_{\mathrm{ETU2}} n_3^2 - W_{\mathrm{CR1}} n_1 n_4 - \frac{n_4}{\tau_4} + W_{\mathrm{nR}}(54) n_5, \quad (7)$$

$$\frac{dn_5}{dt} = K_{\mathrm{ESA2}} n_3 - W_{\mathrm{CR2}} n_1 n_5 - \frac{n_5}{\tau_5}, \quad (8)$$

where $R_P=\sigma_{13}(I_P/h\nu_P)$ is the pump rate (s^{-1}), I_P is the intensity of the pump light in W cm^{-2} and $h\nu_P$ is the photon energy of the pump radiation. β_{ij} represents the luminescence branching ratio and τ_{R_i} is the radiative lifetime of the $^5S_2$, $^5F_5$, $^5I_6$, and $^5I_7$ excited states where i=5, 4, 3, and 2, respectively. The ESA1 pump ratio is given by $K_{\mathrm{ESA1}}=fR_P,f$, the cross section ratio, is given by $f=\sigma_{\mathrm{ESA1}}(\lambda_P)/\sigma_{\mathrm{GSA}}(\lambda_P)$ and λ_P is the pumping wavelength.

B. Numerical solution of the rate equations

It was established by numerical solution of Eqs. (4)–(8) that the ESA2 process does not contribute to the population inversion but depletes it slightly by approximately 5%. As a result of this small contribution, ESA2 process was neglected in the rate equation model for laser pumping near 1100 nm and a saving in the computation time was achieved.

In order to better understand the role of ESA and ETU processes in the operation of singly Ho^{3+}-doped ZBLAN fiber laser systems, we applied the numerical simulation to two Ho^{3+}-doped ZBLAN systems: case 1, fiber laser employing fiber having 4.2 mol % Ho^{3+} pumped at 1100 nm corresponding to the experiment reported in Ref. 13, and, case 2, fiber laser employing fiber having 0.5 mol % Ho^{3+} pumped at 1175 nm which corresponds to the experiment reported in Ref. 23. In the case of the dilute Ho^{3+}-doped ZBLAN system, i.e., case 2, the ETU processes were neglected in the rate equation system because it was established that these processes are important for Ho^{3+} concentrations above 1 mol %.

The results of the numerical simulations of the population inversion (n_3-n_2) between the $^5I_6$ and $^5I_7$ levels for case 1, shown in Fig. 6(a), indicates that the ESA1 pump ratio makes a significant contribution to the system when f

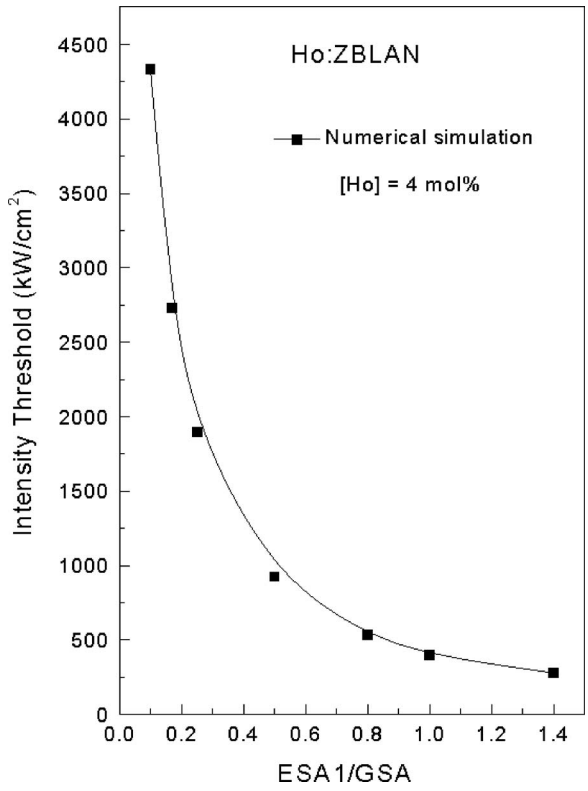

FIG. 7. Calculated pump intensity at the threshold for 2.92 μm laser emission for Ho^{3+} (4 mol %)-doped ZBLAN as a function of the cross section ratio f.

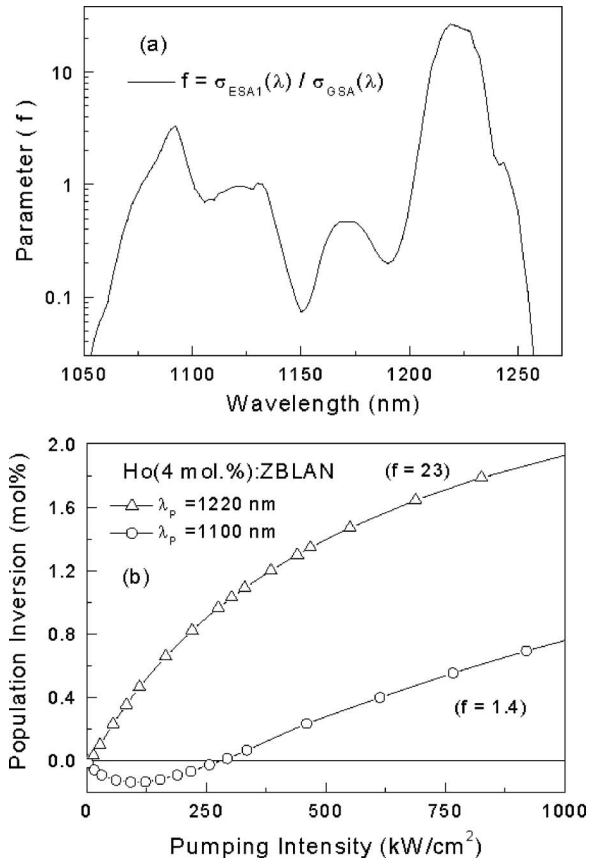

FIG. 8. Calculated (a) cross section ratio $f(\lambda)=\sigma_{ESA1}(\lambda)/\sigma_{GSA}(\lambda)$ as a function of the excitation wavelength and (b) population inversion as a function of the pump rate determined for an excitation wavelength $\lambda_P=1095$ nm and $\lambda_P=1225$ nm for Ho^{3+} (4 mol %)-doped ZBLAN.

$=K_{ESA1}/R_P \geqslant 0.1$, when the processes ETU1, ETU2, ESA1, and CR1 are considered. From these results, we can take the pump rate (or pump intensity) required to produce a zero population inversion for each f value. Figure 7 shows the calculated pump intensity as a function of the f parameter for Ho^{3+} (4 mol %)-doped ZBLAN pumped near 1100 nm.

To determine the importance of ESA1 to the operation of the cw Ho^{3+}-doped ZBLAN fiber laser, case 1, we calculated the pump ratio f as a function of the pump wavelength; the results of which are shown in Fig. 8(a). The one-phonon sideband relevant to the $^5I_7 \rightarrow {}^5I_4$ absorption transition, which increases the f parameter from ~ 0 to ~ 1.4, is important in allowing ESA1 to contribute to the population inversion for excitation near 1100 nm. In contrast, no sideband contribution to ESA1 is necessary for excitation near 1225 nm ($f \sim 23$). The predicted threshold intensity for excitation at 1100 nm was obtained by inspecting the threshold intensity behavior as a function of f near $f \sim 1.4$, as shown in Fig. 7. A threshold intensity of 278 kW cm^{-2} was determined which is approximately 14% smaller than the experimental threshold intensity of ~ 323 kW cm^{-2}.[13] The numerical simulation of the population inversion presented in Fig. 8(b) shows that 2.9 μm fiber laser operation using Ho^{3+} (4 mol %)-doped ZBLAN will be more efficient with a pump wavelength near 1225 nm compared to 1100 nm.

We analyzed the contribution of ETU1 to the population inversion for the case 1 fiber laser for two distinct cases when $f=0.5$: (i) when ETU1 process is on and (ii) when ETU1 process is suppressed (off). Figure 6(b) shows that the pump intensity at threshold increases 1.4 times when ETU1 is switched off in the numerical simulation. Thus, ETU1 contributes to the population inversion, but it cannot sustain the population inversion.

Figure 9 shows the results of the numerical calculation of the population inversion for the two Ho^{3+} laser system cases. The dilute system required a pump intensity of ~ 6 kW cm^{-2} to produce a zero population inversion which is significantly smaller than the highly doped system (~ 278 kW cm^{-2}). In addition, the initial slope efficiency of the fiber laser employing dilute Ho^{3+} concentration fiber was calculated to be ~ 5.3 times higher than the slope efficiency relating to the highly doped system, in partial agreement with the reported results. The performance of the fiber laser employing 4.2 mol % Ho^{3+} was strongly affected by the ETU2 process because it has a comparatively larger rate coefficient as determined from our previous investigation.[16]

V. CONCLUSIONS

We have isolated and quantified two ESA processes that affect the operation of Ho^{3+}-doped ZBLAN fiber lasers that operate on the ~ 3 μm $^5I_6 \rightarrow {}^5I_7$ laser transition when the $^5I_8 \rightarrow {}^5I_6$ GSA process is employed. We have established that the phonon sidebands have been important in recent demonstrations of singly Ho^{3+}-doped ZBLAN fiber lasers when the pump wavelength is not resonant with the ESA processes. We calculated the population inversion between the $^5I_6$ and

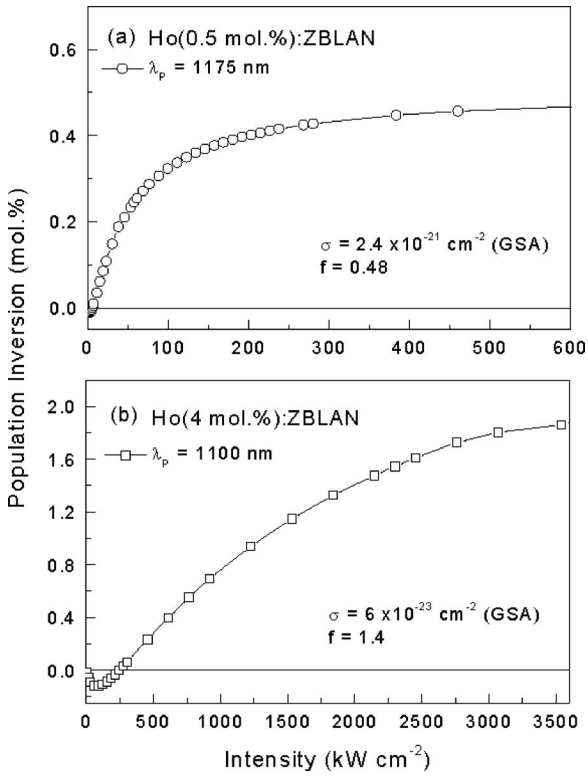

FIG. 9. Calculated steady state population inversion (n_3-n_2) as a function of the pump intensity for (a) Ho^{3+} (0.5 mol %)-doped ZBLAN pumped at 1175 nm and (b) Ho^{3+} (0.5 mol %)-doped ZBLAN pumped at 1100 nm.

$^5I_7$ levels of Ho^{3+} relevant to two experimental demonstrations of 3 μm Ho^{3+}-doped ZBLAN fiber lasers and established that, while the ESA1 process $^5I_7 \rightarrow {}^5I_4$ is responsible for allowing a population inversion to take place, in highly concentrated systems, the ETU process $^5I_6$, $^5I_6 \rightarrow {}^5F_5$, $^5I_8$ seriously impedes the performance. We have shown that the ESA1 process, that depends on the square of the pumping intensity, makes a positive contribution to the population inversion when $K_{\mathrm{ESA1}} \geqslant 0.1R_P$.

ACKNOWLEDGMENTS

The authors thank financial support from FAPESP (Grant Nos. 1995/4166-0 and 2000/10986-0), CNPq, and the Australian Research Council.

[1]D. Gapontsev, Laser Focus World **41**, 9 (2005).
[2]S. Mihashi, G. J. Jako, J. Incze, M. S. Strong, and C. W. Vaughan, Ann. N.Y. Acad. Sci. **267**, 263 (1976).
[3]M. L. Wolbarsht, IEEE J. Quantum Electron. **20**, 1427 (1984).
[4]M. C. Pierce, S. D. Jackson, M. R. Dickinson, T. A. King, and P. Sloan, Lasers Surg. Med. **26**, 495 (2000).
[5]D. K. Killinger, N. Menyuk, and W. E. Defeo, Appl. Phys. Lett. **36**, 402 (1980).
[6]A. Mayer, J. Comera, H. Charpentier, and C. Jaussaud, Appl. Opt. **17**, 391 (1978).
[7]T. M. Taczak and D. K. Killinger, Appl. Opt. **37**, 8460 (1998).
[8]S. D. Jackson, T. A. King, and M. Pollnau, Opt. Lett. **24**, 1133 (1999).
[9]B. Srinivasan, J. Tafoya, and R. K. Jain, Opt. Express **4**, U10 (1999).
[10]T. Sandrock, D. Fischer, P. Glas, M. Leitner, and M. Wrage, Opt. Lett. **24**, 1286 (1999).
[11]S. D. Jackson, Opt. Lett. **29**, 334 (2004).
[12]X. S. Zhu and R. Jain, Opt. Lett. **32**, 26 (2007).
[13]S. D. Jackson, Electron. Lett. **40**, 1400 (2004).
[14]T. Sumiyoshi, H. Sekita, T. Arai, S. Sato, M. Ishihara, and M. Kikuchi, IEEE J. Sel. Top. Quantum Electron. **5**, 936 (1999).
[15]S. D. Jackson, Appl. Phys. Lett. **83**, 1316 (2003).
[16]A. F. H. Librantz, S. D. Jackson, F. H. Jagosich, L. Gomes, G. Poirier, S. J. L. Ribeiro, and Y. Messaddeq, J. Appl. Phys. **101**, 123111 (2007).
[17]R. C. Powell, *Physics of Solid-State Laser Materials* (Springer-Verlag, New York, 1998), pp. 101–103.
[18]C. Li, Y. Guyot, C. Linarès, R. Moncorgé, and M. F. Joubert, OSA Proc. Adv. Solid-State Lasers **15**, 91 (1993).
[19]B. M. Walsh, N. P. Barnes, and B. Di Bartolo, J. Appl. Phys. **83**, 2772 (1998).
[20]L. Wetenkamp, G. F. West, and H. Többen, J. Non-Cryst. Solids **140**, 35 (1992).
[21]L. V. G. Tarelho, L. Gomes, and I. M. Ranieri, Phys. Rev. B **56**, 14344 (1997).
[22]Y. Chen and F. Auzel, J. Non-Cryst. Solids **184**, 278 (1995).
[23]D. V. Talavera and E. B. Mejía, Laser Phys. **16**, 436 (2006).